Volume 13
Number 30
14 August 2022
Pages 4355-4454

Polymer Chemistry

rsc.li/polymers

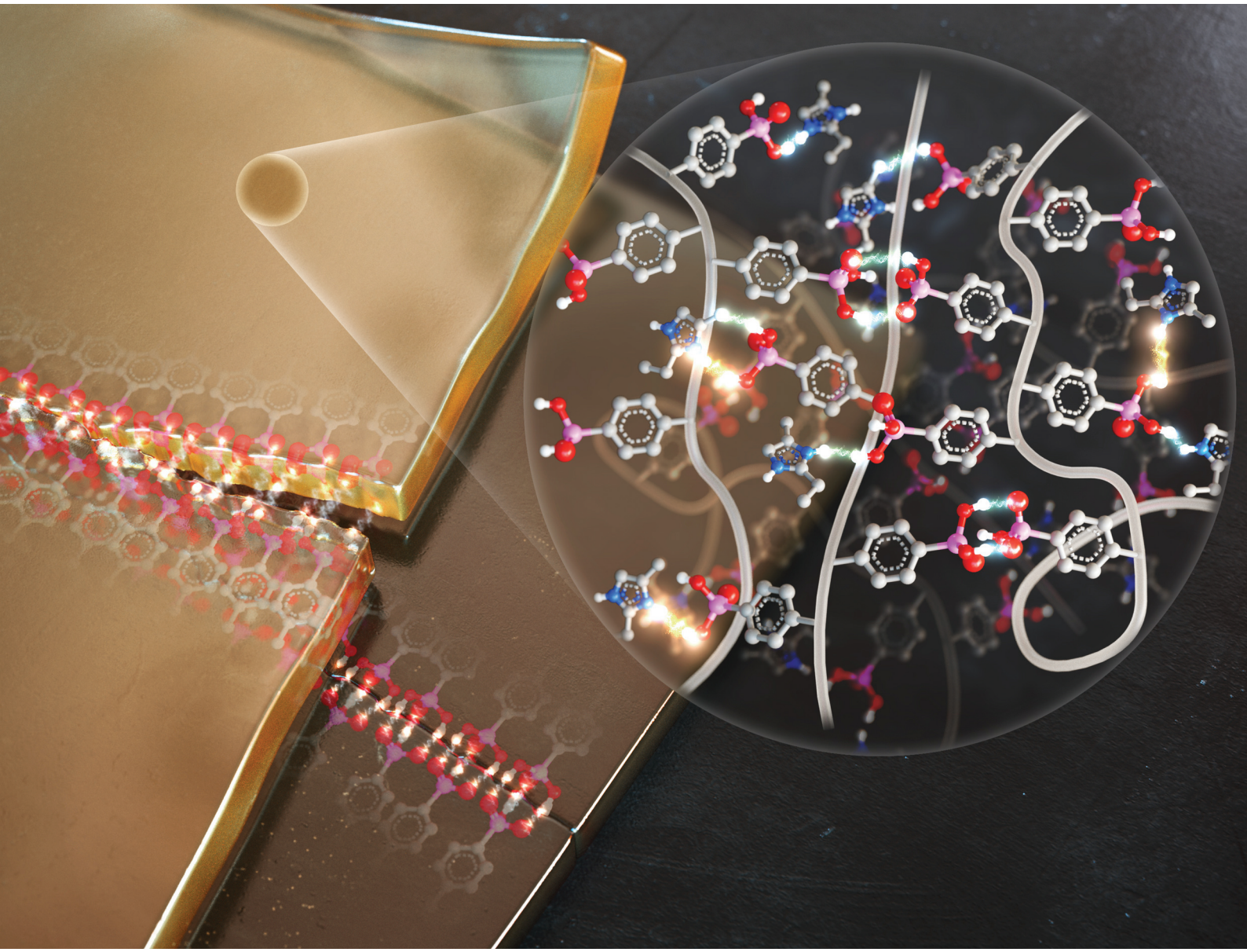

ISSN 1759-9962

ROYAL SOCIETY OF CHEMISTRY

PAPER

Sejong Kang and Moon Jeong Park
Tailoring intermolecular interactions in ion gels with rationally designed phosphonic acid polymers

Polymer Chemistry

ROYAL SOCIETY OF CHEMISTRY

PAPER

View Article Online
View Journal | View Issue

Cite this: *Polym. Chem.*, 2022, **13**, 4372

Tailoring intermolecular interactions in ion gels with rationally designed phosphonic acid polymers†

Sejong Kang and Moon Jeong Park *

Ideal ion gels exhibit high ionic conductivities and mechanical strengths, but developing such ion gels is challenging, as a high ionic conductivity generally requires a high ionic liquid content, which inevitably reduces the mechanical strength. Herein, we report the controlled syntheses of poly(4-styrenephosphonic acid) (PS4P) and poly(3-styrenephosphonic acid) (PS3P) polymers to achieve challenging goals *via* the modulation of intermolecular interactions in ion gels containing ionic liquids. Less steric hindrance and increased rotational freedom in PS4P enabled effective swelling and facilitated self-healing of the PS4P-based block copolymer ion gels *via* robust hydrogen bond formation. Meanwhile, the adjacent chain packing with restricted swelling of the PS3P-based ion gels enabled high toughness and concerted proton hopping. To form dual-crosslinked ion gels, the type of ionic liquid anion was changed to promote ionic interactions, which yielded elastic gels with improved conductivities. Varying the types of ionophobic blocks used in the syntheses of the phosphonated block copolymers allowed the control of the chain stretching in ionic domains. This determined the local ion concentration, thereby modifying the ionic conductivities of the ion gels. Our approach establishes the design of phosphonic acid polymers that exhibit a configurable balance of ionic and hydrogen bonding interactions at the molecular level, which should be a platform for developing advanced ion gels.

Received 19th May 2022,
Accepted 21st June 2022

DOI: 10.1039/d2py00646d

rsc.li/polymers

Introduction

Extensive research has been devoted to the use of polymer electrolytes in batteries,[1,2] fuel cells,[3] sensors,[4,5] actuators,[6,7] and adhesives.[8] The key characteristics of polymer electrolytes in expanding their scope of applications are high ionic conductivities and elasticities, chemical/electrochemical stabilities, and mechanical robustness.[9–13] Among the various types of polymer electrolytes, gel polymer electrolytes exhibit several advantages, such as rapid ion diffusion and facile control of mechanical properties.[14,15] The simple, versatile fabrication processes of gel polymer electrolytes by dispersion of the polymer networks in excess liquid electrolytes are also advantageous, with the mechanical properties determined by the crosslinking densities of the polymer networks and the contents of liquid components.[16,17]

As advanced forms of gel polymer electrolytes, the immobilization of ionic liquids in polymer matrices received considerable attention.[18] These are denoted ion gels (or ionogels), which exhibit considerably reduced leakage of liquid components after long-term use, in addition to lower risks of flammability and volatility. Ion gels may be classified into two broad classes based on the elastic nature of the polymer matrix: chemically[19,20] or physically[21] crosslinked. Given the reversible characteristics of physical crosslinks, network formation *via* hydrogen bonding, π···π stacking, and ion–dipole and Coulomb interactions receives considerable attention.[21–23] The most widely employed polymers in this class are polar polymers, such as poly(vinylidene fluoride-*co*-hexafluoropropylene) (PVDF-HFP),[24,25] polyvinyl alcohol,[5,26] and polyethylene oxide,[27,28] which exhibit ion–dipole interactions with embedded ionic liquids.

Various attempts to control the strengths of the ion–dipole interactions in ion gels are reported.[29] The most intuitive approach is to control ion solvation in polar polymers by changing the type of ionic liquid.[22] Alternatively, the structures of the repeating units in a polymer that can interact with ionic liquids may be varied, *e.g.*, the interactions of the imidazolium and CF_3 units of PVDF-HFP were tuned by adjusting the fraction of HFP.[30] However, the properties of ion gels are complicated by numerous factors, as the crystallinities and dielectric properties of the polymer matrices are also altered by changes in the composition of PVDF-HFP.

Department of Chemistry, Pohang University of Science and Technology (POSTECH), Pohang, Korea 790-784. E-mail: moonpark@postech.ac.kr

† Electronic supplementary information (ESI) available: ^{1}H-NMR and ^{31}P-NMR of monomers and polymers, temperature-dependent FT-IR, and SAXS profiles of ion gels. See DOI: https://doi.org/10.1039/d2py00646d

The use of block copolymers comprising ionophilic and -phobic blocks is another approach,[31] with physical crosslinking occurring selectively in the ionophilic domains and the surrounding ionophobic chains yielding additional mechanical strength *via* entanglement. The self-assembly of block copolymers enables effective immobilization of ionic liquids in nanoscale ionic domains, and morphological control of ion gels enables the facile modulation of ionic conductivity and mechanical properties over a wide range.[14,32] Owing to advances in polymer synthesis, the chemical control of polymer backbones influences the ionic conductivities, mechanical properties, and electrochemical stabilities of copolymer-based ion gels.[33]

Despite considerable synthetic efforts to chemically control physical crosslinking, preparing an ion gel with a high ionic conductivity and mechanical strength is challenging, as the former essentially requires a high ionic liquid content, which inevitably reduces the mechanical strength. *In situ* polymerization of ionic liquids[34,35] or zwitterionic monomers[36] is part of this endeavor to form dense physically crosslinked networks with enhanced mechanical properties, but effective ionic conduction across tightly crosslinked networks remains elusive. In addition, unlike in hydrogels containing excess water, obtaining high degrees of ionization in ion gels is challenging.[37,38]

The formation of double physically crosslinked networks emerged as a promising methodology to achieve the apparently contradictory aims of high ionic conductivity and mechanical strength.[23,33,39] *Via* the covalent attachment of rationally designed functional moieties to the polymer backbone, simultaneous Coulomb and hydrogen bonding interactions were envisaged.[33] In this context, recent studies by Wang *et al.*[40] are notable, as tough, stretchable, and self-healable ion gels were developed *via* the random copolymerization of two functional monomers of acrylamide and acrylic acid. With the addition of ionic liquids, poorly solvated polyacrylamide predominantly formed hydrogen bonds, whereas highly solvated polyacrylic acid enabled ion–ion and –dipole interactions to form networks of ionic bonds. Although this strengthened the elastic properties of the ion gels, control of the intermolecular interactions in such copolymers is nontrivial, with a low potential for diversification of the functional groups of the ionophilic polymer chains.[41]

Herein, we report the syntheses of phosphonated homopolymers and block copolymers based on poly(4-styrenephosphonic acid) (PS4P) and poly(3-styrenephosphonic acid) (PS3P), with phosphonic acid groups bonded at different positions of the styrene units. The aim was to control the strengths of the interchain hydrogen bonding interactions *via* steric hindrance and rotational freedom. Two ionic liquids with different anions were employed in preparing the ion gels to control the balance of ionic and hydrogen bonding interactions. The effects of ion pair formation between the ionic liquid cations and the phosphonate moieties that coexist with interchain hydrogen bonds, *i.e.*, dual-network formation, on the elasticity and ionic conductivity were observed. Further, the effects of the types of ionophobic blocks in the block copolymers on the local concentration of ions at the molecular level, and thus, the ionic conductivities of the ion gels, were also studied.

Experimental

Materials

3-Bromostyrene (97%), 4-bromostyrene (97%), triphenylphosphine (PPh_3, 99%), *N*,*N*-dicyclohexylmethylamine (Cy_2NCH_3, 97%), diethyl phosphite (DEP, 98%), 1-bromoethylbenzene ($C_6H_5CH(CH_3)Br$, 97%), *N*,*N*,*N*′,*N*″,*N*″-pentamethyldiethylenetriamine (PMDETA, 99%), copper(I) bromide (CuBr, 98%), copper(I) chloride (CuCl, ≥99%), bromotrimethylsilane ($(CH_3)_3SiBr$, 97%), isoprene (≥99%), sec-butyllithium (sec-BuLi, 1.4M in cyclohexane), ethylene oxide (EO, ≥99.8%), anisole (99.7%), toluene (99.8%), methanol (MeOH, 99.8%), tetrahydrofuran (THF, ≥99.9%), diethyl ether (anhydrous, ≥99.7%), *p*-toluenesulfonyl hydrazide (TSH, ≥97%), *o*-xylene (97%), α-bromoisobutyryl bromide (BIBB, 98%), triethylamine (TEA, ≥99.5%), acetic acid (≥99%), 2-ethyl-4-methylimidazole (2E4MIm, 95%), and methanesulfonic acid (MsOH, ≥99.0%) were purchased from Sigma-Aldrich. Palladium(II) acetate ($Pd(OAc)_2$, 98%) was purchased from Strem Chemicals, dimethyl phosphate (DMP, 98%) and ethanol (EtOH, ≥95%) were purchased from Thermo Fisher Scientific, and dichloromethane (DCM, 99.5%), ethyl acetate (EA, 99.5%), isopropanol (99.5%), and magnesium sulfate ($MgSO_4$, 99.5%) were purchased from Samchun Chemicals. The ω-hydroxyl-terminated poly(isobutylene) (PIB-OH, M_n = 3.8 kg mol^{-1}) was obtained from Polymer Source. CuBr and CuCl were purified by washing with acetic acid and diethyl ether prior to use. All other chemicals were used as received.

Synthesis of diethyl (3-vinylphenyl)phosphonate and diethyl (4-vinylphenyl)phosphonate monomers

$Pd(OAc)_2$ (0.22 g, 1.0 mmol), PPh_3 (0.78 g, 3.0 mmol), Cy_2NCH_3 (6.4 mL, 30 mmol) and DEP (6.2 mL, 48 mmol) were added to 3-bromostyrene (or 4-bromostyrene) (1.8 g, 10 mmol) in ethanol (60 mL) under an argon atmosphere. The mixtures were refluxed at 80 °C with stirring for 48 h. After the reaction was terminated by lowering the temperature to 25 °C, the mixtures were dried. After extracting aqueous phases using DCM/distilled water, the monomers were dried on $MgSO_4$ and separated by silica gel column chromatography (DCM : EA = 4 : 1). ^{1}H and ^{31}P nuclear magnetic resonance (NMR) spectra of monomers were recorded on Bruker instruments. Diethyl (3-vinylphenyl)phosphonate ^{1}H NMR (500 MHz, $CDCl_3$) δ_H (ppm): 7.79–7.84 (d, 1H, Ph), 7.61–7.68 (m, 1H, Ph), 7.53–7.56 (d, 1H, Ph), 7.35–7.42 (m, 1H, Ph), 6.64–6.74 (m, 1H, CH_2=C**H**), 5.76–5.81 (d, 1H, C**H$_2$**=CH), 5.27–5.31 (d, 1H, C**H$_2$**=CH), 3.98–4.18 (m, 4H, 2 × –OC**H$_2$**CH_3), 1.26–1.31 (t, 6H, 2 × –OCH_2C**H$_3$**). ^{31}P NMR (203 MHz, $CDCl_3$) δ_P (ppm): 16.64. Diethyl (4-vinylphenyl)phosphonate ^{1}H NMR (500 MHz, $CDCl_3$) δ_H (ppm): 7.72–7.79 (m, 2H, Ph), 7.45–7.49 (m, 2H, Ph), 6.66–6.76 (m, 1H, CH_2=C**H**), 5.81–5.86 (d, 1H, C**H$_2$**=CH), 5.34–5.37 (d, 1H, C**H$_2$**=CH), 3.98–4.19 (m, 4H, 2 ×

–OC**H**$_2$CH$_3$), 1.27–1.32 (t, 6H, 2 × –OCH$_2$C**H**$_3$). ^{31}P NMR (203 MHz, $CDCl_3$) δ_P (ppm): 16.69.

Synthesis of poly(3-diethylphosphonated styrene) (PS3DEP) and poly(4-diethylphosphonated styrene) (PS4DEP)

PS3DEP (or PS4DEP) were synthesized by atom transfer radical polymerization (ATRP) of diethyl vinylbenzylphosphonate monomer (0.55 g, 3 mmol), CuBr catalyst (0.014 g, 0.1 mmol), PMDETA (41.7 μL, 0.2 mmol) and 1-bromoethylbenzene initiator (13.6 μL, 0.1 mmol) in anisole (50 wt% to the monomer). The reaction mixtures were refluxed at 90 °C under an argon environment, and terminated when the conversion rate reaches ~60% to yield a polymer with degree of polymerization of ~20. After terminating the reaction by cooling the reactor to 25 °C, the catalyst was removed by passing the mixtures through neutral alumina using DCM. The residual reagents were eliminated by membrane dialysis against THF/water (2/1 vol/vol) and methanol with regenerated cellulose membrane having molecular weight cutoff of 1.0 kg mol^{-1} (MWCO-1.0), followed by vacuum drying at 40 °C for a week. PS3DEP ^{1}H NMR (500 MHz, $CDCl_3$) δ_H (ppm): 6.13–7.65 (br, n × 4H, Ph), 3.75–4.17 (br, 2n × 2H, –OC**H**$_2$CH$_3$), 1.37–2.1 (br, n × 3H, –C**H**$_2$C**H**–), 1.05–1.37 (br, 2n × 3H, –OCH$_2$C**H**$_3$). ^{31}P NMR (203 MHz, $CDCl_3$) δ_P (ppm): 16.49. PS4DEP ^{1}H NMR (500 MHz, $CDCl_3$) δ_H (ppm): 6.18–7.81 (br, n × 4H, Ph), 3.89–4.35 (br, 2n × 2H, –OC**H**$_2$CH$_3$), 1.41–2.35 (br, n × 3H, –C**H**$_2$C**H**–), 1.10–1.41 (br, 2n × 3H, –OCH$_2$C**H**$_3$). ^{31}P NMR (203 MHz, $CDCl_3$) δ_P (ppm): 16.69.

Synthesis of poly(methylbutylene) (PMB) and PIB macroinitiators

For the preparation of PMB macroinitiator, the ω-hydroxy-terminated polyisoprene (PI-OH) was first synthesized by anionic polymerization of isoprene in cyclohexane using sec-BuLi as an initiator and EO as a terminating agent. Then, 3 molar equivalents of TSH to the number of PI repeating units were added to the PI-OH in *o*-xylene (80 wt% to TSH), followed by stirring at 135 °C for 12 h. After cooling down the reaction mixtures to 25 °C, solid precipitates were removed by filtration, and obtained solution was dried. The product was purified by repeated precipitations in methanol/isopropanol = 3/1 (vol/vol) to yield the ω-hydroxyl terminated PMB (PMB-OH). The molecular weight of PMB-OH was determined to be M_n = 3.4 kg mol^{-1} by end-group analysis using ^{1}H NMR. Narrow molecular weight distribution of PMB-OH with polydispersity index (PDI) of 1.05 was confirmed by size exclusion chromatography (SEC, Waters Breeze 2 HPLC) using polystyrene standards in THF eluent. In order to synthesize the PMB and PIB macroinitiators for ATRP, PMB-OH (3.4 g, 1.0 mmol) or PIB-OH (3.8 g, 1.0 mmol) was mixed with TEA (4.2 mL, 30 mmol) in 40 mL of DCM. Under an argon environment, BIBB (1.2 mL, 8 mmol) was added dropwise to the solution at 0 °C, and stirred at 25 °C for 12 h. Remaining salts and the excess of BIBB were removed by extracting aqueous phases of the mixtures using DCM/distilled water. The PMB-BIBB (or PIB-BIBB) macroinitiator was recovered by vacuum drying for a week. PMB-BIBB ^{1}H NMR (500 MHz, $CDCl_3$) δ_H (ppm): 4.11–4.28 (m, 2H, –C**H**$_2$O–), 1.96 (s, 6H, –COC(C**H**$_3$)$_2$Br), 0.94–1.61 (br, m × 5H, –C**H**$_2$C**H**(CH$_3$)C**H**$_2$–), 0.52–0.94 (br, m × 3H, CH$_2$CH(C**H**$_3$)CH$_2$–). PIB-BIBB ^{1}H NMR (500 MHz, $CDCl_3$) δ_H (ppm): 3.83–4.07 (m, 2H, –C**H**$_2$O–), 1.97 (s, 6H, –COC(C**H**$_3$)$_2$Br), 1.30–1.56 (br, m × 2H, –C**H**$_2$C(CH$_3$)$_2$–), 0.81–1.30 (br, m × 6H, –CH$_2$C(C**H**$_3$)$_2$–).

Synthesis of PMB-*b*-PS3DEP, PMB-*b*-PS4DEP, PIB-*b*-PS3DEP and PIB-*b*-PS4DEP block copolymers

A set of PMB-*b*-PS3DEP, PMB-*b*-PS4DEP, PIB-*b*-PS3DEP and PIB-*b*-PS4DEP block copolymers were synthesized by ATRP of diethyl 3- or 4-vinylbenzylphosphonate using CuCl/PMDETA catalyst and PMB-BIBB (or PIB-BIBB) macroinitiator in toluene (50 wt% to monomers). The reaction mixtures were refluxed at 90 °C under an argon atmosphere. After termination, catalyst was removed by passing through neutral alumina with DCM. The residual reagents were eliminated by membrane dialysis (MWCO-1.0) against THF/water (2/1 vol/vol) and methanol. The block copolymers were obtained by vacuum drying at 40 °C for a week. PMB-*b*-PS3DEP ^{1}H NMR (500 MHz, $CDCl_3$) δ_H (ppm): 6.08–7.68 (br, n × 4H, Ph), 3.73–4.20 (br, 2n × 2H, –OC**H**$_2$CH$_3$), 1.41–2.26 (br, n × 3H, –C**H**$_2$C**H**–), 1.13–1.41 (br, m × 5H, –C**H**$_2$C**H**(CH$_3$)C**H**$_2$–), 0.91–1.13 (br, 2n × 3H, –OCH$_2$C**H**$_3$), 0.55–0.91 (br, m × 3H, CH$_2$CH(C**H**$_3$)CH$_2$–). ^{31}P NMR (203 MHz, $CDCl_3$) δ_P (ppm): 18.56. PMB-*b*-PS4DEP ^{1}H NMR (500 MHz, $CDCl_3$) δ_H (ppm): 6.19–7.86 (br, n × 4H, Ph), 3.91–4.41 (br, 2n × 2H, –OC**H**$_2$CH$_3$), 1.60–2.35 (br, n × 3H, –C**H**$_2$C**H**–), 1.16–1.60 (br, m × 5H, –C**H**$_2$C**H**(CH$_3$)C**H**$_2$–), 0.99–1.16 (br, 2n × 3H, –OCH$_2$C**H**$_3$), 0.59–0.99 (br, m × 3H, CH$_2$CH(C**H**$_3$)CH$_2$–). ^{31}P NMR (203 MHz, $CDCl_3$) δ_P (ppm): 18.60. PIB-*b*-PS3DEP ^{1}H NMR (500 MHz, $CDCl_3$) δ_H (ppm): 6.15–7.78 (br, n × 4H, Ph), 3.73–4.24 (br, 2n × 2H, –OC**H**$_2$CH$_3$), 1.69–2.35 (br, n × 3H, –C**H**$_2$C**H**–), 1.35–1.53 (br, m × 2H, –C**H**$_2$C(CH$_3$)$_2$–), 1.17–1.35 (br, 2n × 3H, –OCH$_2$C**H**$_3$), 0.64–1.17 (br, m × 6H, –CH$_2$C(C**H**$_3$)$_2$–). ^{31}P NMR (203 MHz, $CDCl_3$) δ_P (ppm): 18.81. PIB-*b*-PS4DEP ^{1}H NMR (500 MHz, $CDCl_3$) δ_H (ppm): 6.15–7.81 (br, n × 4H, Ph), 3.91–4.35 (br, 2n × 2H, –OC**H**$_2$CH$_3$), 1.60–2.25 (br, n × 3H, –C**H**$_2$C**H**–), 1.39–1.60 (br, m × 2H, –C**H**$_2$C(CH$_3$)$_2$–), 1.21–1.39 (br, 2n × 3H, –OCH$_2$C**H**$_3$), 0.71–1.21 (br, m × 6H, –CH$_2$C(C**H**$_3$)$_2$–). ^{31}P NMR (203 MHz, $CDCl_3$) δ_P (ppm): 18.59.

Synthesis of PS3P, PS4P, PMB-*b*-PS3P, PMB-*b*-PS4P, PIB-*b*-PS3P and PIB-*b*-PS4P block copolymers

After dissolving DEP-capped phosphonated polymers in anhydrous chloroform (80 wt% to monomers), the 20 molar equivalents of bromotrimethylsilane to the number of phosphonate groups were added dropwise to the solution at 0 °C. The mixtures were slowly heated to 40 °C and stirred for 24 h to yield trimethylsilane-capped phosphonated polymers. After removing solvents by argon blowing, excessive amount of methanol was added to the reactor and stirred at 25 °C for 8 h to obtain the polymers in acid form. The phosphonic acid polymers were recovered by vacuum drying at 40 °C for a week. PS3P ^{1}H NMR (500 MHz, methanol-d_4) δ_H (ppm): 6.54–7.86 (br, n × 4H, Ph), 1.28–2.55 (br, n × 3H, –C**H**$_2$C**H**–). ^{31}P NMR (203 MHz, methanol-d_4) δ_P (ppm): 14.97. PS4P ^{1}H NMR (500 MHz, methanol-d_4) δ_H (ppm): 6.41–7.85 (br, n × 3H, Ph), 1.22–2.43 (br, n ×

3H, –C**H**$_2$C**H**–). ^{31}P NMR (203 MHz, methanol-d_4) δ_P (ppm): 14.92. PMB-*b*-PS3P ^{1}H NMR (500 MHz, methanol-d_4) δ_H (ppm): 6.54–7.84 (br, n × 4H, Ph), 0.94–1.56 (br, m × 5H, –C**H**$_2$C**H**(CH_3)C**H**$_2$–), 0.51–0.94 (br, m × 3H, CH_2CH(C**H**$_3$)CH_2–). ^{31}P NMR (203 MHz, methanol-d_4) δ_P (ppm): 16.74. PMB-*b*-PS4P ^{1}H NMR (500 MHz, methanol-d_4/THF-d_8) δ_H (ppm): 6.30–7.90 (br, n × 3H, Ph), 0.93–1.48 (br, m × 5H, –C**H**$_2$C**H**(CH_3)C**H**$_2$–), 0.50–0.93 (br, m × 3H, CH_2CH(C**H**$_3$)CH_2–). ^{31}P NMR (203 MHz, methanol-d_4/THF-d_8) δ_P (ppm): 16.89. PIB-*b*-PS3P ^{1}H NMR (500 MHz, methanol-d_4/THF-d_8) δ_H (ppm): 6.58–7.71 (br, n × 4H, Ph), 1.39–1.57 (br, m × 2H, –C**H**$_2$C(CH_3)$_2$–), 0.76–1.23 (br, m × 6H, –CH_2C(C**H**$_3$)$_2$–). ^{31}P NMR (203 MHz, methanol-d_4/THF-d_8) δ_P (ppm): 17.08. PIB-*b*-PS4P ^{1}H NMR (500 MHz, methanol-d_4/THF-d_8) δ_H (ppm): 6.25–7.89 (br, n × 4H, Ph), 1.38–1.61 (br, m × 2H, –C**H**$_2$C(CH_3)$_2$–), 0.75–1.22 (br, m × 6H, –CH_2C(C**H**$_3$)$_2$–). ^{31}P NMR (203 MHz, methanol-d_4/THF-d_8) δ_P (ppm): 17.08.

Preparation of ion gels comprising phosphonic acid polymers and ionic liquids

Nonstoichiometric ionic liquids with 2/1 molar ratio of 2E4MIm/DMP (or 2E4MIm/MsOH) were prepared. Predetermined amounts of the ionic liquids were immobilized into phosphonic acid polymers using anhydrous THF/methanol (3/1 vol/vol). The ion gels were fabricated by solvent casting at 40 °C, followed by vacuum drying at 50 °C for a week. All sample preparations were performed inside an argon-filled glove box to avoid the issue of water contamination. Fourier transform infrared spectroscopy (FT-IR) spectra of neat polymers, neat ionic liquids, and ion gels were recorded using the attenuated total reflection prism (PerkinElmer) with resolution of 4 cm^{-1}.

Morphological analysis

Under the argon-filled glove box, the neat polymers and ion gels were loaded into homemade airtight aluminum cells covered by Kapton windows. Synchrotron small-angle and wide-angle X-ray scattering (SAXS and WAXS) experiments were performed in the PLS-II 9A and 4C beamlines at Pohang Accelerator Laboratory, equipped with two-dimensional detector. The incident X-ray beam wavelength (λ) was 0.063 nm ($\Delta\lambda/\lambda = 10^{-4}$). In order to investigate microphase separated morphologies and local chain structures, different sample-to-detector distances of 2, 0.5 and 0.2 m were employed. Scattering intensities as a function of scattering vector were obtained by circularly averaging of the two-dimensional scattering data.

Thermal and mechanical properties

Thermal properties of neat ionic liquids and ion gels were investigated by differential scanning calorimetry (DSC, Q20, TA Instruments) and thermogravimetric analysis (TGA, Q50, TA Instruments). 10 mg of samples were loaded in aluminum pans and thermograms were recorded at heating/cooling rates of 10 °C min^{-1}. Dynamic storage and loss moduli of ion gels were measured with heating/cooling rates of 2 °C min^{-1}, strain of 0.1% and a frequency of 0.5 rad s^{-1} in the stress-controlled mode using a Discovery HR-20 rheometer (TA Instruments), equipped with a parallel plate of 8 mm diameter. Stress–strain curves of ion gel membranes were measured using UTM (ST-1003, SALT) under ambient conditions (RH = ~30%) with a drag speed of 2 mm min^{-1} and resolution of 2 mN.

Ionic conductivity measurements

Inside an argon-filled glove box, using an ac impedance spectroscopy (VersaStat3, Princeton Applied Research), through-plane ionic conductivities of the ion gels were measured in frequency range of 1–100 000 Hz and temperature window of 30–150 °C. Stainless steels (2.0 cm × 2.0 cm) were used as blocking electrodes and 135 μm-thick Kapton film with a hole diameter of 0.5 cm was used as a spacer.

Results and discussion

Syntheses of polymers with phosphonic acid functional groups at different positions

As a strategy to control the strengths of hydrogen bonding interactions in ion gels, two types of polymers with phosphonic acid functional groups at different positions were synthesized in homo- and block architectures *via* ATRP. As shown in Scheme 1a, the monomers of diethyl 3- and 4-vinylbenzylphosphonate were first synthesized *via* the Pd-catalyzed cross-coupling of 3- or 4-bromostyrene precursors, respectively, with DEP. The ^{1}H- and ^{31}P-NMR spectra of each monomer are shown in Fig. S1.† PS3DEP and PS4DEP were obtained *via* ATRP and narrow molecular weight distributions with PDIs of <1.08 were confirmed by SEC (Fig. S2†). The degree of polymerization (DP) of each polymer was determined using ^{1}H-NMR based on the integrals of the end group and diethyl group in the repeating unit (Fig. S2†).

After hydrolysis, the acidic forms of the phosphonate polymers, PS3P and PS4P, are obtained. The complete elimination of the ethoxy groups without self-condensation of the P–OH moieties was confirmed using ^{1}H- and ^{31}P-NMR (see ESI for details, Fig. S3†). For the syntheses of the phosphonated block copolymers, two macroinitiators based on PMB and PIB were prepared, as shown in Scheme 1b and c, respectively (see ESI for details, Fig. S4–S6†). Only the hydrogenated form of the major PI isomer was shown as the chemical structure of PMB. The main aim of varying the type of ionophobic block is to adjust the segregation strengths[42] of the microphase-separated structures, which may affect the conformations of the PS4P and PS3P chains under confinement. The molecular weights of PMB and PIB are 3.4 and 3.8 kg mol^{-1}, respectively. Using ATRP, four sets of block copolymers of PMB-*b*-PS3DEP, PMB-*b*-PS4DEP, PIB-*b*-PS3DEP, and PIB-*b*-PS4DEP were synthesized, and subsequent hydrolysis yielded the corresponding acid forms of the block copolymers: PMB-*b*-PS3P, PMB-*b*-PS4P, PIB-*b*-PS3P, and PIB-*b*-PS4P. Hereafter, we collectively refer to the phosphonated polystyrene as PSP.

As shown in Table 1, the DPs of PSP within the block copolymers were targeted to be 10, 20, and 30 at fixed molecular

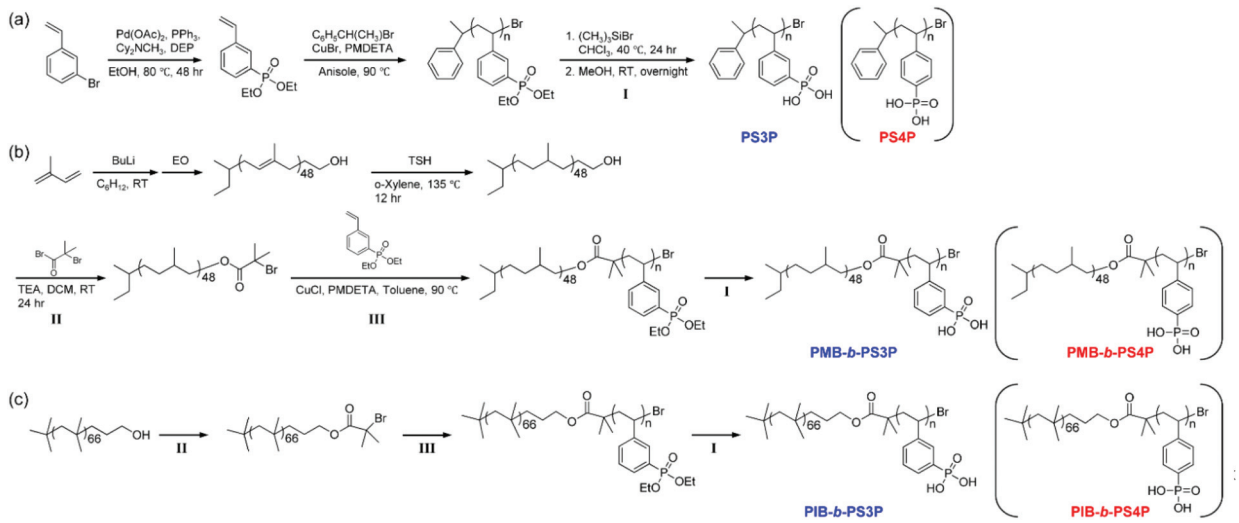

Scheme 1 Synthetic routes to the preparation of polymers having phosphonic acid functional groups at different positions in (a) homo and (b and c) block architectures by employing PMB and PIB as macroinitiators.

weights of ionophobic blocks to systematically control the volume fraction of the PSP block. This yields 12 block copolymers, which display low PDIs. Representative ^{1}H- and ^{31}P-NMR spectra of PMB-*b*-PS3DEP, PMB-*b*-PS4DEP, PMB-*b*-PS3P, and PMB-*b*-PS4P, with DPs of 20 (PS3P) and 22 (PS4P), are shown in Fig. 1a and b, respectively (see ESI for NMR spectra of PIB-based block copolymers, Fig. S7 and S8†). Notably, in the ^{1}H-NMR spectra of the PS3DEP-containing block copolymers, upfield chemical shifts with peak broadening,[43] representing ethoxy groups, are observed when compared with the spectra of the PS4DEP-based samples. This indicates steric hindrance of neighboring ethoxy moieties and the polymer backbone. Representative SEC profiles of PMB-*b*-PS3DEP, PMB-*b*-PS4DEP, PIB-*b*-PS3DEP, and PIB-*b*-PS4DEP samples with similar DPs are shown in Fig. 1c.

Morphologies of phosphonated polymers

We investigated the local structures and chain conformations of the phosphonated polymers using WAXS experiments.

Table 1 Phosphonated polymers used in this study

Polymer	DP of PSP	MW (kg mol^{-1})	PDI	ϕ_{PSP}
PS3P	20	3.7	1.07	1
PS4P	15	2.8	1.08	1
	9	3.4–1.7	1.09	0.24
PMB-*b*-PS3P	20	3.4–3.7	1.06	0.41
	30	3.4–5.5	1.08	0.51
	8	3.8–1.5	1.16	0.21
PIB-*b*-PS3P	19	3.8–3.5	1.10	0.39
	30	3.8–5.5	1.11	0.50
	9	3.4–1.7	1.08	0.24
PMB-*b*-PS4P	22	3.4–4.1	1.06	0.44
	32	3.4–5.9	1.07	0.53
	10	3.8–1.8	1.15	0.25
PIB-*b*-PS4P	17	3.8–3.1	1.10	0.36
	30	3.8–5.5	1.13	0.50

Fig. 2a shows the representative WAXS profiles of the PS4P and PS3P homopolymers, which were measured at 25 °C and are essentially independent of temperature. For PS4P and PS3P, similar ion cluster peaks are observed at ~4.0 nm^{-1} (indicated by shadows),[41] corresponding to spacings of ~1.6 nm, but the backbone-to-backbone (q_1) and ring-to-ring (q_2) correlations differ significantly. As schematically depicted in the right-hand panels of Fig. 2a, overall, the PS3P chains exhibit closer backbone stacking (d_1, 1.16 nm) and adjacent ring arrangements (d_2, 0.44 nm), compared with those of the PS4P chains at 1.40 and 0.49 nm, respectively. We also observe a broad shoulder in the wide-angle range (q_3) for PS4P only, reflecting interchain $-PO_3H_2$ correlation distances of ~0.35 nm. This indicates strong interchain hydrogen bonding interactions in PS4P, which are weakened in less-organized PS3P.

Closer backbone–backbone and ring–ring stacking in the absence of interchain PO_3H_2–PO_3H_2 correlations are consistently observed for the PS3P-containing block copolymers. Remarkably, as shown in Fig. 2b, the q_1 signals of the PS4P chains strengthen for PIB-*b*-PS4P and PMB-*b*-PS4P, compared with the weak q_1 signals of the PS3P-based block copolymers. This suggests that the PS4P chains are more structured upon confinement by the ionophobic blocks. Notably, the ion cluster peaks of the PS3P chains are substantially weakened when they are bonded to ionophobic blocks. Suppressed ion aggregations in congested PS3P domains *via* confinement are envisioned. It is also noteworthy that the PIB chain packing (0.62 nm) is considerably larger than the PMB chain correlation (0.47 nm).

The dissimilar strengths of the hydrogen bonding interactions in PS4P and PS3P were examined using FT-IR spectroscopy. As shown in Fig. 2c, the characteristic bands of the phosphonic acid groups are observed in the wavenumber range 1190–850 cm^{-1}. The stretching vibration of the P–OH band of PS4P is shifted to a lower wavenumber at 924 cm^{-1},

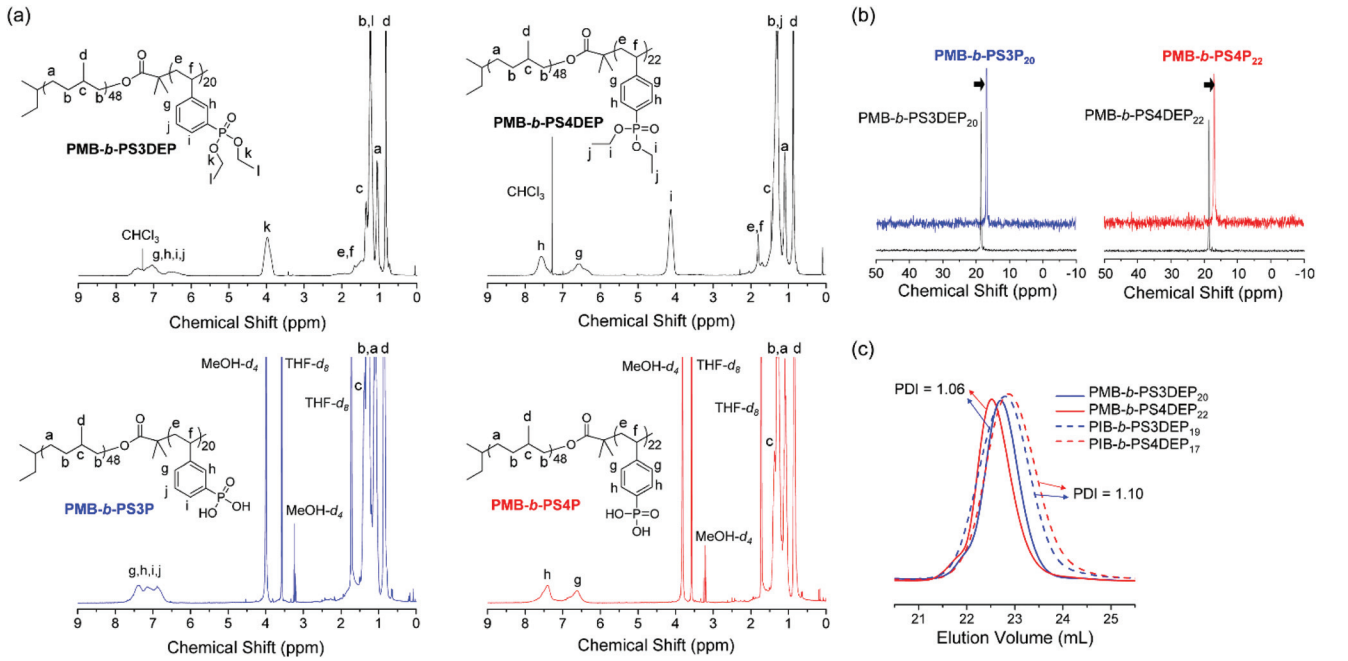

Fig. 1 Representative (a) ^{1}H-NMR and (b) ^{31}P-NMR spectra of PMB-*b*-PS3DEP and PMB-*b*-PS4DEP (before hydrolysis), and PMB-*b*-PS3P and PMB-*b*-PS4P (after hydrolysis). (c) SEC traces of four sets of PMB-*b*-PS3DEP, PMB-*b*-PS4DEP, PIB-*b*-PS3DEP, and PIB-*b*-PS4DEP with similar DPs of PSDEP blocks.

with an enhanced absorbance compared with that at 936 cm^{-1} in the spectrum of PS3P. A strong absorbance of the P═O band at ~1150 cm^{-1} is also observed for PS4P.[44] This indicates that the positions of the phosphonic acid groups on the polymer backbone are crucial in controlling the hydrogen bonding interactions of the phosphonated polymers, with the hydrogen bonding interactions in PS4P strengthened.

Different chain conformations of PS4P and PS3P yield dissimilar microphase-separated morphologies of their block copolymers.

Fig. 3a shows representative SAXS profiles of PMB-*b*-PS4P and PMB-*b*-PS3P, with PSP units with DPs of 9 (DP of PMB is fixed at 48 for all PMB-based block copolymers). For PMB-*b*-PS3P, a lamellar (LAM) structure with Bragg peaks (▼) at q^*, $2q^*$, $3q^*$, and $4q^*$ is observed, whereas for PMB-*b*-PS4P, a hexagonal cylindrical (HEX) structure coexists with the LAM structure, as indicated by a series of Bragg peaks (⇓) at q^*, $\sqrt{3}q^*$, $\sqrt{4}q^*$, $\sqrt{7}q^*$, $\sqrt{9}q^*$, $\sqrt{12}q^*$... and those (∇) at q^*, $2q^*$, $3q^*$, and $4q^*$. The domain size of the HEX structure is approximately 11% larger than that of the LAM structure, which is attributed the interfacial curvature that balances the stretching of PS4P chains in PMB-*b*-PS4P.[45,46]

Further, when PIB is used as an ionophobic block instead of PMB, the domain sizes of the LAM and HEX structures increase significantly. Fig. 3b and c show the representative SAXS profiles of the PIB-*b*-PS3P and PMB-*b*-PS3P block copolymers with PSP units with various DPs. For block copolymers with relatively short PS3P chains, as shown in Fig. 3b, PIB-*b*-$PS3P_8$ and PMB-*b*-$PS3P_9$ display LAM morphologies with Bragg peaks at q^*, $2q^*$, $3q^*$, and $4q^*$, but the segregation strength of

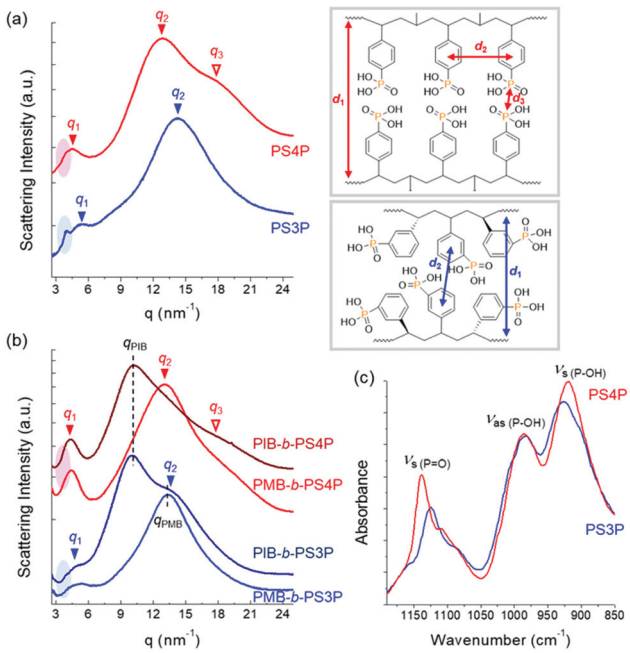

Fig. 2 WAXS profiles of (a) PS4P and PS3P homopolymers and (b) their block copolymers: ion cluster peaks (shadows), backbone-to-backbone (q_1), ring-to-ring (q_2), and interchain $-PO_3H_2$ (q_3) correlations. Scattering profiles are vertically shifted for clarity. Schematics drawn in the right panel of (a) show dissimilar chain arrangements of PS4P and PS3P. (c) FT-IR spectra of PS4P and PS3P in the wavenumber range of 1190–850 cm^{-1}.

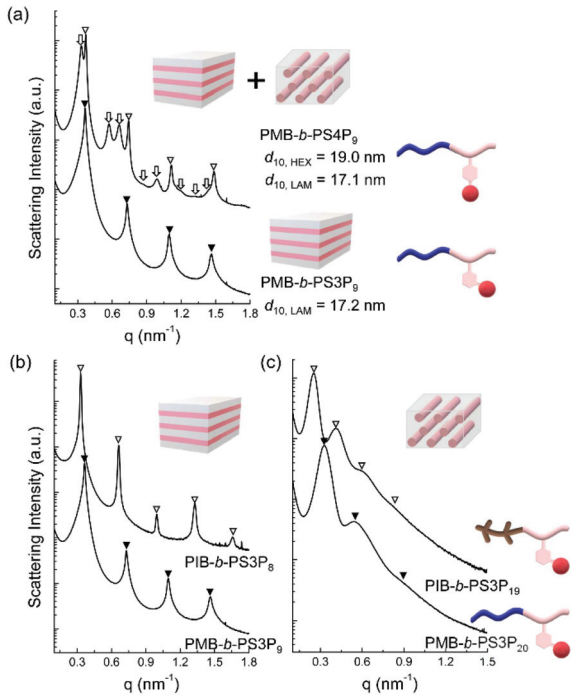

Fig. 3 (a) SAXS profiles of PMB-*b*-PS4P$_9$ and PMB-*b*-PS3P$_9$ block copolymers. For PMB-*b*-PS4P$_9$, coexistence of HEX and LAM structures are shown, whereas only LAM structure was observed for PMB-*b*-PS3P$_9$. SAXS profiles of (b) PIB-*b*-PS3P$_8$ and PMB-*b*-PS3P$_9$, and (c) PIB-*b*-PS3P$_{19}$ and PMB-*b*-PS3P$_{20}$ block copolymers, indicative of LAM and HEX structure, respectively. Schematic illustrations of the self-assembled morphology and chemical structure of each block copolymer are shown in (a–c). All scattering profiles were measured at 25 °C.

PIB-*b*-PS3P$_8$ is enhanced compared with that of PMB-*b*-PS3P$_9$, yielding narrow peak widths. The domain size of PIB-*b*-PS3P$_8$ increases by approximately 10%, despite its similar molecular weight, which is attributed to the largely dissimilar backbone-to-backbone stacking distances of the PIB and PMB chains (Fig. 2b). Remarkably, the LAM structure persists despite the large change in domain size, unlike the HEX structure that is observed for PMB-*b*-PS4P.

A similar pattern is also observed for PIB-*b*-PS3P$_{19}$ and PMB-*b*-PS3P$_{20}$ with relatively long PS3P chains, which exhibit HEX morphologies with Bragg peaks at q^*, $\sqrt{3}q^*$, $\sqrt{4}q^*$..., as shown in Fig. 3c. PIB-*b*-PS3P$_{19}$ again displays a better-resolved morphology with a significantly increased domain size of 32% compared with those of PMB-*b*-PS3P$_{20}$. In terms of intermolecular interactions and local ion concentrations in the PSP domains, this suggests the potential weakening of ionic and hydrogen bond interactions in PIB-*b*-PSP block copolymers *via* chain stretching.

Ion gels fabricated using the phosphonated polymers and ionic liquids

Ion gels were prepared by embedding predetermined amounts of ionic liquids into the phosphonated polymers. To modulate the balance of electrostatic and hydrogen bonding interactions in the samples, various anionic moieties were used in the ionic liquids: DMP and MsOH, with 2E4MIm as the common cationic moiety. As PSP polymers possess phosphonic acid groups in their repeating units, a nonstoichiometric ionic liquid with a 2/1 molar ratio of 2E4MIm/DMP (or 2E4MIm/MsOH) was employed for the cation–anion charge balance. Thermal properties of ion gels were examined by TGA and DSC experiments (Fig. S9†).

Because of the low acidity of DMP (pK_a = ~2), which is similar to that of the Ph–PO$_3$H$_2$ unit, hydrogen bonding interactions likely prevail in ion gels fabricated using 2E4MIm/DMP. However, MsOH, with a pK_a of approximately −2, should enable ionic interactions of MsO$^-$···2E4MIm$^+$ and Ph-PO$_3$H$^-$···2E4MIm$^+$ in 2E4MIm/MsOH-containing PSP gels, which coexist with the hydrogen bonds of the remaining neutral moieties, facilitating the formation of dual networks. The top panels of Fig. 4a schematically show the dissimilar intermolecular interactions in ion gels comprising the PSP polymers and different ionic liquids.

The intermolecular interactions in the ion gels were investigated using FT-IR spectroscopy. As shown in the bottom panels of Fig. 4a, several distinct changes in the IR spectra of the ion gels (solid lines) are observed in the region 1190–875 cm^{-1} compared with those of the neat PMB-*b*-PS3P and PMB-*b*-PS4P block copolymers (dotted lines). With embedded 2E4MIm/DMP, the stretching vibration of the P–OH band, ν(P–OH), is reduced, indicating weakened hydrogen bonding interactions of the PSP chains upon deprotonation. However, stronger hydrogen bonding interactions are observed for the PMB-*b*-PS4P gels compared to those of the PMB-*b*-PS3P analogs, as indicated by the absorbance of ν(P–OH). The reductions in ν(P–OH) absorbances are more pronounced for the gels containing 2E4MIm/MsOH, and simultaneously, the appearance of strong stretching vibrations representing the PO$_3$ bands are observed.[44] Based on the shifts in wavenumber to lower values, the formation of resonance-stabilized PO$_3$ bound to the 2E4MIm$^+$ cation may occur within the 2E4MIm/MsOH-containing gels.

The ionic interactions in PMB-*b*-PSP containing 2E4MIm/MsOH result in densely packed ionic domains, as indicated by their lower degrees of swelling compared to those of their 2E4MIm/DMP-containing counterparts. Fig. 4b shows the scattering profiles of PMB-*b*-PS4P$_9$ and PMB-*b*-PS3P$_9$ with 2E4MIm/DMP or 2E4MIm/MsOH. For comparison, those of the neat block copolymers are shown as dotted profiles in each plot. With 2E4MIm/DMP, the LAM peaks (▼) of PMB-*b*-PS3P$_9$ are weakened, and the HEX structure (⇓) becomes dominant, along with a considerable increase in the domain size. Only the HEX structure is observed for PMB-*b*-PS4P$_9$ containing 2E4MIm/DMP, indicating that the hydrogen bond networks in 2E4MIm/DMP-containing PS4P form extended chain structures. The chemical similarity of DMP with the –PO$_3$H$_2$ group also improves the miscibility of 2E4MIm/DMP with the PSP chains to yield effective chain stretching. This is not observed for the ion gels fabricated with 2E4MIm/MsOH, with PMB-*b*-PS3P$_9$ less prone to swelling due to its conserved LAM struc-

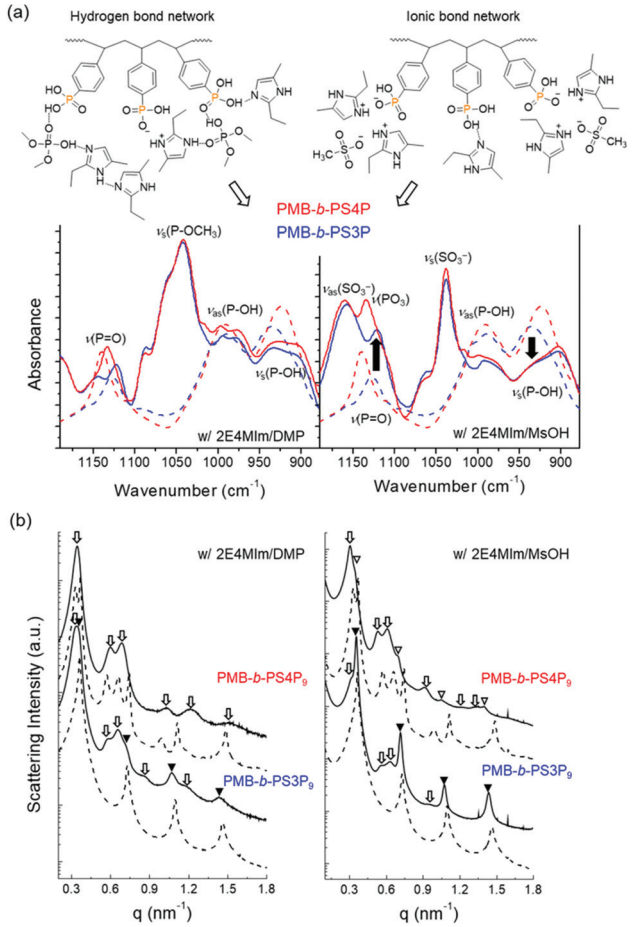

Fig. 4 (a) Schemes representing intermolecular interactions and FT-IR spectra of PMB-*b*-PS4P (red) and PMB-*b*-PS3P (blue) comprising different ionic liquids. The IR spectra of neat block copolymer are also shown by dotted lines for a comparison. (b) SAXS profiles of PMB-*b*-PS4P and PMB-*b*-PS3P with embedded 2E4MIm/DMP or 2E4MIm/MsOH. Dotted lines are the scattering profiles of neat block copolymers. Bragg peaks of HEX (⇓) and LAM (∇ and ▼) structures are indicated in the figure. All data were measured at 25 °C.

ture (▼), indicating that ionic bonds are formed in the congested PS3P domains. PMB-*b*-PS4P$_9$ exhibits a prevalent HEX structure (⇓), with a considerable increase in the domain size of ~20% and traces of coexisting LAM structures (∇).

Notably, the strengths of the hydrogen bonding interactions in the ion gels could be altered by changing the temperature. Overall, heating the ion gels resulted in increases in ν(P–OH) absorbance, whereas the $\nu(PO_3)$ band remained unchanged at 90 °C (Fig. S10†). The PSP–PSP interchain hydrogen interactions could be amplified as the temperature was increased above the glass transition temperature (T_g), but the degree of deprotonation of $-PO_3H_2$ groups was not significantly affected in the temperature range of interest. This suggested that the thermodynamics of PSP-based ion gels could be tuned by two types of intermolecular interactions with different temperature dependencies, which should essentially be connected to changes in the elasticities of ion gels with temperature.

Our hypotheses regarding the ionic liquid-dependent swelling behaviors and temperature-dependent intermolecular interactions of the PSP-based ion gels were confirmed by rheological experiments. Because of the brittle characteristics of PSP homopolymers, fabrication of PSP ion gels into self-standing membranes was not trivial. We therefore focused on block copolymer ion gels for reliable rheological measurements.

Fig. 5a and b show the storage (G') and loss moduli (G'') in the temperature range 25–100 °C for PMB-*b*-PS3P$_9$ and PMB-*b*-PS4P$_9$ containing 2E4MIm/MsOH or 2E4MIm/DMP. Intriguing differences in the rheological properties of the samples are observed, depending on the type of ionic liquid. With 2E4MIm/MsOH, the PMB-*b*-PS3P$_9$ and -PS4P$_9$ gels are elastic at room temperature, which is attributed to the dual physically crosslinked networks formed by the ionic and hydrogen bonding interactions. The densely packed PSP chains also contribute to the elasticities of the PMB-*b*-PSP ion gels *via* electrostatic interactions. When the sample temperature is increased to $>T_g$ (~50 °C) values of the ion gels, the elastic behaviors are no longer observed, with $G' \approx G''$.

The introduction of 2E4MIm/DMP into PMB-*b*-PS3P$_9$ or PMB-*b*-PS4P$_9$ results in higher moduli than those of the respective 2E4MIm/MsOH counterpart. The G' of PMB-*b*-PS4P$_9$

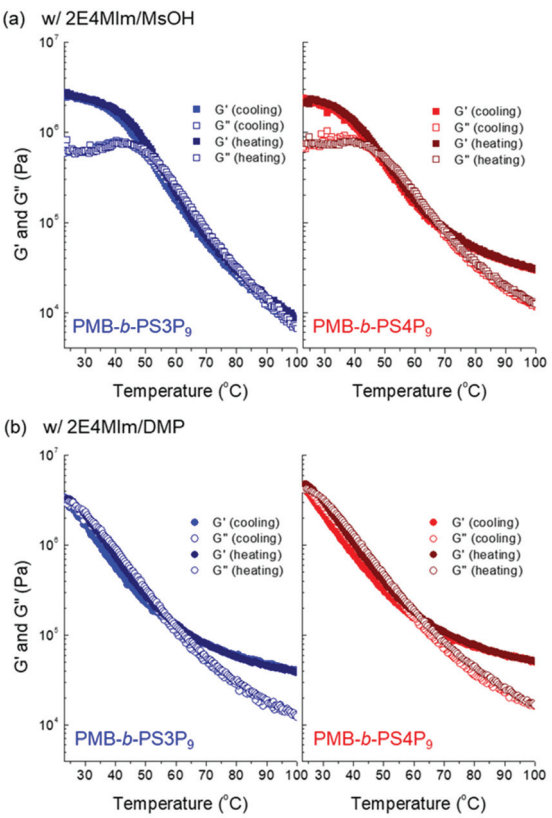

Fig. 5 Storage (G', filled symbols) and loss (G'', open symbols) moduli of (a) PMB-*b*-PS3P$_9$ and PMB-*b*-PS4P$_9$ comprising different ionic liquids: (a) 2E4MIm/MsOH and (b) 2E4MIm/DMP. Data were acquired during cooling/heating scans at a rate of 2 °C min^{-1}, strain of 0.1% and a frequency of 0.5 rad s^{-1}.

containing 2E4MIm/DMP is >2-fold larger than that obtained using 2E4MIm/MsOH. Despite the increased moduli, the loss tangent values of both ion gels with 2E4MIm/DMP are ~1 at 25 °C. This indicates the rubbery states of the samples, which are remarkable, as neat 2E4MIm/MsOH (2/1) and 2E4MIm/DMP (2/1) are liquids with low viscosities at room temperature. The G' of 2E4MIm/DMP-containing PMB-*b*-PS4P$_9$ is approximately 1.4-fold higher than that of the PMB-*b*-PS3P$_9$ analog owing to effective hydrogen bond formation in the PS4P domains. Thus, the mechanical properties of ion gels comprising phosphonated block copolymers and ionic liquids may be largely controlled by tailored intermolecular interactions in the ionic domains.

Heating of the ion gels results in rapid reductions in their moduli, but their elasticities simultaneously increase, leading to $G' > G''$ for the ion gels containing 2E4MIm/DMP at elevated temperatures (Fig. 5b). The strengthened PSP–PSP interchain hydrogen bonding interactions with increasing temperature should explain this observation. The remarkable re-entrant elastic properties with heating observed for PMB-*b*-PS4P$_9$ containing 2E4MIm/MsOH may also be understood in the same context.

Tensile studies of ion-gel membranes with thicknesses of ~200 μm were conducted to investigate their elastic and plastic behaviors with respect to the type of ionic liquid used. As shown in Fig. 6a, PMB-*b*-PS3P$_9$ and PMB-*b*-PS4P$_9$ with embedded 2E4MIm/MsOH exhibit high moduli of 17 and 12 MPa, respectively, owing to the development of dual-cross-linked networks. The gel membranes fracture when strains of >5% are applied, suggesting that the electrostatic interactions in the ion gels enable elasticity with enhanced tensile strength, but the entangled chains formed *via* ion aggregation are susceptible to mechanical deformation. Conversely, the 2E4MIm/DMP-based gels display improved toughness with broadened plastic regions owing to dominant hydrogen bonding interactions in the PSP domains, enabling chain elongation by disrupting the hydrogen bonds. PMB-*b*-PS3P$_9$ gel membranes with 2E4MIm/DMP are stretchable up to a strain of 11%. The calculated moduli of the PMB-*b*-PS4P$_9$ and PMB-*b*-PS3P$_9$ membranes at low strains of <0.5% are 9.5 and 6.0 MPa, respectively.

Fig. 6b shows images of PMB-*b*-PS3P$_9$ gel membranes fabricated using 2E4MIm/DMP. Approximately 350 μm-thick membranes were cut in half, and then the surfaces of each piece were annealed at room temperature. Repeated pulling and bending deformations of the self-healed membranes reveal non-noticeable fracture generation, in sharp contrast to the 2E4MIm/MsOH-containing gels, which exhibit brittle characteristics. Notably, self-healing rapidly accelerates with increasing temperature (*i.e.*, 90 °C), which facilitates interchain hydrogen bond formation. When the gel membranes are damaged, the cracks readily heal at room temperature, as shown in Fig. 6c. Self-healing is considerably faster for 2E4MIm/DMP-containing PMB-*b*-PS4P$_9$ than for the PMB-*b*-PS3P$_9$ counterparts, owing to the efficient hydrogen bond formation within PMB-*b*-PS4P$_9$.

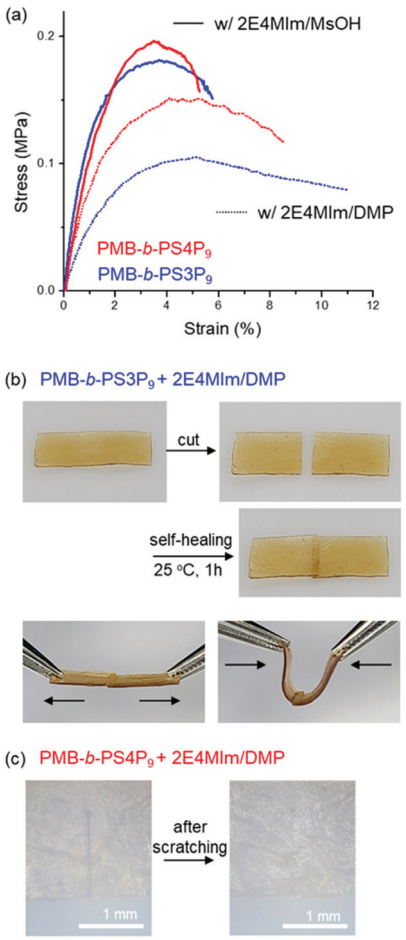

Fig. 6 (a) Stress–strain curves of ion gel membranes measured under ambient conditions. (b) Repeated pulling and bending deformation of self-healed PMB-*b*-PS3P$_9$ comprising 2E4MIm/DMP. (c) Self-healing of damaged PMB-*b*-PS4P$_9$ membranes containing 2E4MIm/DMP.

Role of ionophobic blocks in modulating ion gel characteristics

When the ionophobic polymer is changed from PMB to PIB in synthesizing the phosphonated block copolymers, *i.e.*, PIB-*b*-PS3P and PIB-*b*-PS4P, the formation of hydrogen bond networks with 2E4MIm/DMP is again observed. The formation of elastic gels containing 2E4MIm/MsOH owing to the formation of ionic bond networks is also observed. In addition to these similarities, several noticeable differences are observed in the PIB-*b*-PSP ion gels due to the inherently stretched polymer chains of the neat PIB-*b*-PSP block copolymers (Fig. 3), *e.g.*, the domain size of PIB-*b*-PS3P$_8$ with 2E4MIm/MsOH is 20.7 nm (LAM), and those of PMB-*b*-PS3P$_9$ with 2E4MIm/MsOH are 19.7 (HEX) and 17.6 nm (LAM) (Fig. S11†). Despite the considerably increased domain size, the LAM-to-HEX transition does not occur in PIB-*b*-PS3P$_8$ containing 2E4MIm/MsOH.

The phase diagrams of four sets of phosphonated block copolymers with three different DPs (10, 20, and 30) of PSP units with embedded ionic liquids are shown in Fig. 7. All observed morphologies are thermally stable in the temperature

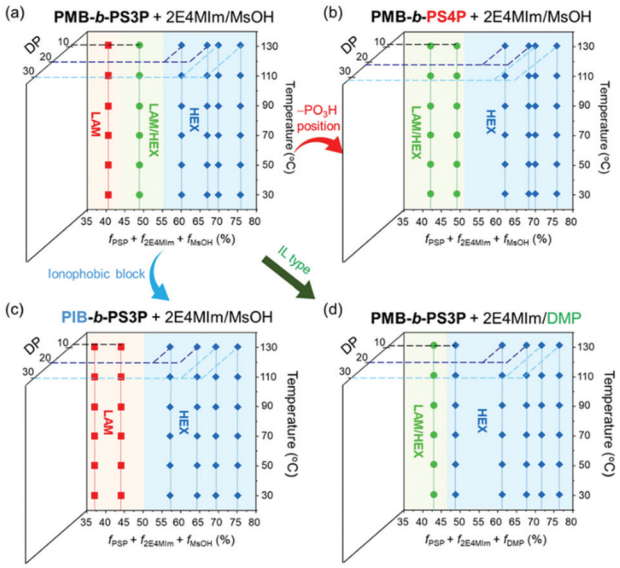

Fig. 7 Phase diagrams of (a) PMB-*b*-PS3P + 2E4MIm/MsOH, (b) PMB-*b*-PS4P + 2E4MIm/MsOH, (c) PIB-*b*-PS3P + 2E4MIm/MsOH, and (d) PMB-*b*-PS3P + 2E4MIm/DMP with three different DPs (10, 20, and 30) of PSP.

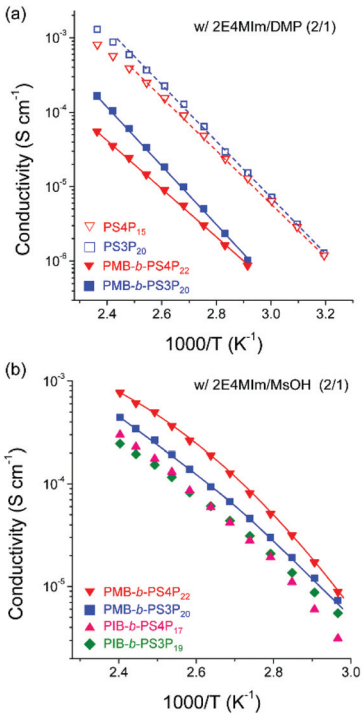

Fig. 8 Temperature-dependent ionic conductivities of (a) 2E4MIm/DMP-containing ion gels with PS4P, PS3P, PMB-*b*-PS4P, and PMB-*b*-PS3P, and those of (b) 2E4MIm/MsOH-containing ion gels with PMB-*b*-PS4P, PMB-*b*-PS3P, PIB-*b*-PS4P, and PIB-*b*-PS3P. The solid and dotted lines in (a) were obtained by Arrhenius fits, whereas the solid lines in (b) were the results of VTF analysis.

range 25–130 °C. In contrast to the least swollen PMB-*b*-PS3P containing 2E4MIm/MsOH (Fig. 7a), the change in the tethered location of the $-PO_3H_2$ group from the *meta*- to the *para*-position of the styrene ring results in shifts in the phase boundaries to widen the HEX phases with 2E4MIm/MsOH (Fig. 7b).

When the ionophobic block is changed from PMB to PIB while preserving the same PS3P block, the LAM structures are stabilized, despite significant changes in domain sizes with embedded 2E4MIm/MsOH (Fig. 7c and Fig. S11†). Because enhanced segregation strengths of microphase-separated morphologies are inferred for PIB-*b*-PSP based on the results of SAXS, poor thermodynamic incompatibility of PIB chains with PSP chains is expected. As the thickness of the PSP domain is increased with the same amount of ionic liquid, charge dilution should occur to yield less organized arrangements of ionic moieties in the PSP domains of PIB-*b*-PSP. When 2E4MIm/MsOH is replaced with 2E4MIm/DMP, effective swelling of the PSP domains stabilizes the HEX structures of all ion gels (Fig. 7d). The PS4P-based samples generally exhibit increased swelling, resulting in LAM-to-HEX transitions even at small volume fractions of ionic phases.

We then examined the temperature-dependent ionic conductivities of the PSP homopolymers and PMB-*b*-PSP block copolymers containing 2E4MIm/DMP in the temperature range 40–150 °C. Representative conductivity data of samples with analogous PSP DPs of approximately 20 are shown in Fig. 8a. Evidently, the PS3P-based samples exhibit higher ionic conductivities than those of the PS4P analogs, with the conductivity difference of the block copolymer samples more pronounced. Based on the linear relationship of conductivity and temperature, proton hopping across hydrogen bond networks in 2E4MIm/DMP-containing PSP domains is likely a dominant ion conduction mechanism, which appears to be accelerated in densely packed PS3P domains. Nevertheless, the PMB-*b*-PS4P samples display advantages in lowering the activation barrier of proton conduction, as determined by Arrhenius fits (77 and 63 kJ mol^{-1} for PMB-*b*-$PS3P_{20}$ and PMB-*b*-$PS4P_{22}$, respectively),[47] by forming effective hydrogen bond networks in the PS4P domains.

For the phosphonated block copolymer gels fabricated using 2E4MIm/MsOH, as shown in Fig. 8b, the conductivity tendency is reversed, with the PMB-*b*-PS4P gels displaying higher conductivities than those of the PMB-*b*-PS3P analogs. This is particularly notable, as the moduli of the PMB-*b*-PS4P gels are higher than those of the PMB-*b*-PS3P samples (Fig. 5b), as the fortified ionic interactions in the PSP domains with 2E4Mlm/MsOH decrease the efficiency of the vehicular diffusion of ions in more congested PS3P domains. In addition, a linear relationship between the conductivity and temperature is no longer observed. The activation energies obtained by Vogel–Tammann–Fulcher (VTF) fits[47] were 485 and 523 K for PMB-*b*-$PS3P_{20}$ and PMB-*b*-$PS4P_{22}$, respectively.

Overall, the conductivity of PSP-based ion gels was lower than conventional crosslinked ion gels,[19] but it is interesting to note that PMB-*b*-PS4P ion gels with 2E4MIm/MsOH showed the conductivity of $>10^{-4}$ S cm^{-1} at a mechanical strength of ~50 kPa without the need for chemical crosslinking.

The types of ionophobic blocks in the phosphonated block copolymers exhibit crucial effects on the ion transport of the ion gels. As shown in Fig. 8b, the PIB-based samples exhibit considerable decreases in ionic conductivity compared with those of the PMB-based samples. The large domains of the PIB-*b*-PSP block copolymers (Fig. 3) may reduce the local concentrations of ions and increase the separation of the ionic sites *via* chain stretching to lower the ionic conductivity. The inherently higher PDI of PIB compared to that of anionically polymerized PMB may cause the heterogeneous widths of the ionophobic domains to increase the packing frustration. We are unaware of the effect of these phenomena on the ion transport properties.

The conclusion reached for 2E4MIm/MsOH-containing ion gels could also be applied to gels fabricated using polar solvents, *e.g.*, when the gels were prepared using phosphonated polymers and DMSO (50/50 wt%), a higher conductivity was observed with PMB-*b*-PS4P than that observed with PMB-*b*-PS3P, and considerable reductions in conductivities were again observed for the PIB-based samples (Fig. S12†). This could be attributed to the prevailing ionic interactions in the gels with high-dielectric-constant solvents. This study highlights the significance of the rational design of ion gels to advance gel properties, which may be tuned by precise chemical and physical control of intermolecular interactions at the molecular level.

Conclusions

Ion gels comprising phosphonated polymers and ionic liquids were investigated. Two main strategies were proposed to simultaneously improve the ion transport and mechanical properties of ion gels. First, the controlled syntheses of PS4P and PS3P in homopolymer and block architectures were performed by varying the degrees of polymerization of the PSP units. The type of ionophobic block was also varied between PMB and PIB in the synthesis of the block copolymer to yield two types of PSP homopolymers and 12 types of PSP-based block copolymers. Second, two different nonstoichiometric ionic liquids, 2E4MIm/DMP and 2E4MIm/MsOH, were employed to fabricate ion gels to strengthen the hydrogen bonding and ionic interactions, respectively. The following conclusions were drawn: (1) when hydrogen bonding interactions prevailed in the ion gels containing 2E4MIm/DMP, the toughness of the ion gels increased with self-healing properties, and heating of the gels resulted in improvement of elastic properties. PMB-*b*-PS3P containing 2E4MIm/DMP exhibited an enhanced ionic conductivity owing to concerted proton hopping across the densely packed PS3P domains. (2) When ion pair formation was promoted using 2E4MIm/MsOH, dual-crosslinked networks were formed, thereby improving the moduli and elasticities of the ion gels. In this case, ion conduction followed vehicular diffusion and was more efficient in the PS4P domains. (3) The segregation strength of phosphonated block copolymers, namely, PSP chain stretching was tuned by the type of ionophobic blocks. This modulated the local ion concentration to affect the ionic conductivities of the ion gels.

Author contributions

M. J. P. conceived the idea and designed the project. S. K. carried out the experiments and analyzed data. M. J. P. and S. K. wrote the paper.

Conflicts of interest

There are no conflicts to declare.

Acknowledgements

This work was supported by the National Research Foundation of Korea (NRF) grant funded by the Korea government (MEST) (No. NRF-2022R1A2C300466711) and by the Korea government (MSIT) (No. NRF-2017R1A5A1015365). We also acknowledge financial support from the Creative Materials Discovery Program through the NRF funded by Ministry of Science and ICT (2018M3D1A1058624).

Notes and references

1 W. H. Meyer, *Adv. Mater.*, 1998, **10**, 439–448.
2 L. Long, S. Wang, M. Xiao and Y. Meng, *J. Mater. Chem. A*, 2016, **4**, 10038–10069.
3 N. Asano, M. Aoki, S. Suzuki, K. Miyatake, H. Uchida and M. Watanabe, *J. Am. Chem. Soc.*, 2006, **128**, 1762–1769.
4 L. M. Zhang, Y. He, S. Cheng, H. Sheng, K. Dai, W. J. Zheng, M. X. Wang, Z. S. Chen, Y. M. Chen and Z. Suo, *Small*, 2019, **15**, 1804651.
5 H. Cheng, B. Wang, K. Yang and C. Wang, *J. Mater. Chem. C*, 2021, **9**, 1014–1024.
6 N. Terasawa, K. Mukai and K. Asaka, *J. Mater. Chem.*, 2012, **22**, 15104–15109.
7 O. Kim, H. Kim, U. H. Choi and M. J. Park, *Nat. Commun.*, 2016, **7**, 13576.
8 Y. Guo, X. Qu, Z. Hu, J. Zhu, W. Niu and X. Liu, *J. Mater. Chem. A*, 2021, **9**, 13597–13607.
9 H. Li, H. Zhang, X. Liao, R. Sun and M. Xie, *Polym. Chem.*, 2020, **11**, 3322–3331.
10 P. Cao, B. Li, G. Yang, S. Zhao, J. Townsend, K. Xing, Z. Qiang, K. D. Vogiatzis, A. P. Sokolov, J. Nanda and T. Saito, *Macromolecules*, 2020, **53**, 3591–3601.
11 V. Bocharova and A. P. Sokolov, *Macromolecules*, 2020, **53**, 4141–4157.
12 C. F. N. Marchiori, R. P. Carvalho, M. Ebadi, D. Brandell and C. M. Araujo, *Chem. Mater.*, 2020, **32**, 7237–7246.
13 G. Bai, N. Liu, C. Wang, W. Wei, X. Liu and Y. Li, *Chem. Commun.*, 2021, **57**, 11493–11496.

14 T. P. Lodge and T. Ueki, *Acc. Chem. Res.*, 2016, **49**, 2107–2114.
15 H. Srour, M. Leocmach, V. Maffeis, A. C. Ghogia, S. Denis-Quanquin, N. Taberlet, S. Manneville, C. Andraud, C. Bucher and C. Monnereau, *Polym. Chem.*, 2016, **7**, 6608–6616.
16 M. M. Mok, X. Liu, Z. Bai, Y. Lei and T. P. Lodge, *Macromolecules*, 2011, **44**, 1016–1025.
17 S. Ida, H. Kitanaka, T. Ishikawa, S. Kanaoka and Y. Hirokawa, *Polym. Chem.*, 2018, **9**, 1701–1709.
18 M. A. Susan, T. Kaneko, A. Noda and M. Watanabe, *J. Am. Chem. Soc.*, 2005, **127**, 4976–4983.
19 Y. Gu, S. Zhang, L. Martinetti, K. H. Lee, L. D. McIntosh, C. D. Frisbie and T. P. Lodge, *J. Am. Chem. Soc.*, 2013, **135**, 9652–9655.
20 H. Li, Z. Feng, K. Zhao, Z. Wang, J. Liu, J. Liu and H. Song, *Nanoscale*, 2019, **11**, 3689–3700.
21 Y. Zhang, L. Chang, P. Sun, Z. Cao, Y. Chen and H. Liu, *RSC Adv.*, 2020, **10**, 7424–7431.
22 S. Chen, B. Zhang, N. Zhang, F. Ge, B. Zhang, X. Wang and J. Song, *ACS Appl. Mater. Interfaces*, 2018, **10**, 5871–5879.
23 W. Zhang, B. Wu, S. Sun and P. Wu, *Nat. Commun.*, 2021, **12**, 4082.
24 S. Yeon, K. Kim, S. Choi, J. Cha and H. Lee, *J. Phys. Chem. B*, 2005, **109**, 17928–17935.
25 G. P. Pandeyab and S. A. Hashmi, *J. Mater. Chem. A*, 2013, **1**, 3372–3378.
26 Y. H. Jo, B. Zhou, K. Jiang, S. Li, C. Zuo, H. Gan, D. He, X. Zhou and Z. Xue, *Polym. Chem.*, 2019, **10**, 6561–6569.
27 S. Ketabi and K. Lian, *Electrochim. Acta*, 2013, **103**, 174–178.
28 S. Song, M. Kotobuki, F. Zheng, C. Xu, S. V. Savilov, N. Hu, L. Lu, Y. Wang and W. D. Z. Li, *J. Mater. Chem. A*, 2017, **5**, 6424–6431.
29 Y. Zhang, M. Li, B. Qin, L. Chen, Y. Liu, X. Zhang and C. Wang, *Chem. Mater.*, 2020, **32**, 6310–6317.
30 Y. Cao, T. G. Morrissey, E. Acome, S. I. Allec, B. M. Wong, C. Keplinger and C. Wang, *Adv. Mater.*, 2017, **29**, 1605099.
31 S. Zhang, K. H. Lee, J. Sun, C. D. Frisbie and T. P. Lodge, *Macromolecules*, 2011, **44**, 8981–8989.
32 R. L. Weber, Y. Ye, A. L. Schmitt, S. M. Banik, Y. A. Elabd and M. K. Mahanthappa, *Macromolecules*, 2011, **44**, 5727–5735.
33 P. Guo, A. Su, Y. Wei, X. Liu, Y. Li, F. Guo, J. Li, Z. Hu and J. Sun, *ACS Appl. Mater. Interfaces*, 2019, **11**, 19413–19420.
34 S. A. Alexandre, G. G. Silva, R. Santamaría, J. P. C. Trigueiro and R. L. Lavall, *Electrochim. Acta*, 2019, **299**, 789–799.
35 C. Zhang, Y. Zhang, Q. Zhao and Z. Xue, *Polym. Chem.*, 2021, **12**, 5631–5639.
36 A. J. D'Angelo and M. J. Panzer, *Chem. Mater.*, 2019, **31**, 2913–2922.
37 O. Rud, T. Richter, O. Borisov, C. Holm and P. Kosovan, *Soft Matter*, 2017, **13**, 3264–3274.
38 S. Panja, A. Seddon and D. J. Adams, *Chem. Sci.*, 2021, **12**, 11197–11203.
39 Z. Li, J. Wang, R. Hu, C. Lv and J. Zheng, *Macromol. Rapid Commun.*, 2019, **40**, 1800776.
40 M. Wang, P. Zhang, M. Shamsi, J. L. Thelen, W. Qian, V. K. Truong, J. Ma, J. Hu and M. D. Dickey, *Nat. Mater.*, 2022, **21**, 359–365.
41 S. Jang, S. Y. Kim, H. Y. Jung and M. J. Park, *Macromolecules*, 2018, **51**, 1120–1128.
42 M. W. Matsen and F. S. Bates, *Macromolecules*, 1996, **29**, 1091–1098.
43 P. R. Schleyer, M. Manoharan, Z. Wang, B. Kiran, H. Jiao, R. Puchta and N. J. Hommes, *Org. Lett.*, 2001, **3**, 2465–2468.
44 R. Luschtinetz, G. Seifert, E. Jaehne and H. P. Adler, *Macromol. Symp.*, 2007, **254**, 248–253.
45 J. Melenkevitz and M. Muthukumar, *Macromolecules*, 1991, **24**, 4199–4205.
46 I. Gunkel and T. Thurn-Albrecht, *Macromolecules*, 2012, **45**, 283–291.
47 U. H. Choi, M. Lee, S. Wang, W. Liu, K. I. Winey, H. W. Gibson and R. H. Colby, *Macromolecules*, 2012, **45**, 3974–3985.